Published in final edited form as:

Biochemistry. 2018 April 17; 57(15): 2266–2277. doi:10.1021/acs.biochem.8b00070.

MxiN Differentially Regulates Monomeric and Oligomeric Species of the *Shigella* Type Three Secretion System ATPase Spa47

Heather B. Case[1] and **Nicholas E. Dickenson**[1,*]

[1]Department of Chemistry and Biochemistry, Utah State University, Logan, UT 84322

Abstract

Shigella rely entirely on the action of a single type three secretion system (T3SS) to support cellular invasion of colonic epithelial cells and to circumvent host immune responses. The ATPase Spa47 resides at the base of the *Shigella* needle-like type three secretion apparatus (T3SA), supporting protein secretion through the apparatus and providing a likely means for native virulence regulation by *Shigella* and a much needed target for non-antibiotic therapeutics to treat *Shigella* infections. Here, we show that MxiN is a differential regulator of Spa47 and that its regulatory impact is determined by the oligomeric state of the Spa47 ATPase, with which it interacts. Both *in vitro* and *in vivo* characterization find that MxiN interaction with Spa47 requires the six N-terminal residues of Spa47 that are also necessary for stable Spa47 oligomer formation and activation. This interaction with MxiN negatively influences the activity of Spa47 oligomers while upregulating the ATPase activity of monomeric Spa47. Detailed kinetic analyses of monomeric and oligomeric Spa47 in the presence and absence of MxiN uncover additional mechanistic insights into the regulation of Spa47 by MxiN, suggesting that the MxiN/Spa47 species resulting from interaction with monomeric and oligomeric Spa47 are functionally distinct and that both could be involved in *Shigella* T3SS regulation. Uncovering Spa47 regulation by MxiN addresses an important gap in the current understanding of how *Shigella* controls T3SA activity and provides the first description of differential T3SS ATPase regulation by a native T3SS protein.

Graphical Abstract

*To whom correspondence should be addressed: Department of Chemistry and Biochemistry, Utah State University, Logan, UT 84322, 0300 Old Main Hill, Logan, UT 84321, Tel. 435-797-0982, nick.dickenson@usu.edu.

Notes:

The authors declare no competing financial interest.

The X Y data sets for Figures 3, 5, and S5 are indexed in OpenAIRE (DOI:10.5281/zenodo.1202232).

Supporting Information Available: Clustal omega multiple sequence alignment and secondary structure prediction profiles of several proposed MxiN homologs (Figure S1), analytical ultracentrifugation analyses of MxiN and Spa47$^{\Delta 1\text{-}6}$ (Figure S2), BSA negative controls for Spa47/MxiN titrations shown in Figure 6A (Figure S3), co-expression and co-purification of MxiN with full-length and truncated Spa47 constructs (Figure S4), and substrate-dependent ATPase activity of the co-expressed and co-purified MxiN$_2$Spa47 complex (Figure S5).

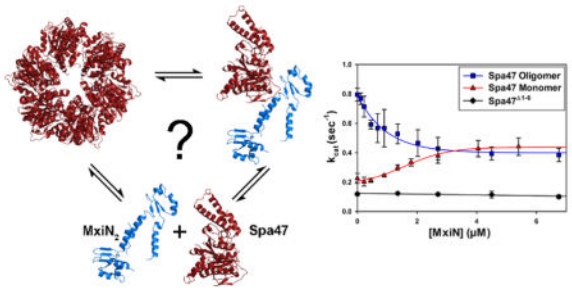

Keywords

Type 3 Secretion System; T3SS; Spa47; ATPase; AAA+; virulence regulation; oligomerization

Introduction

Diarrheal disease is the leading cause of malnutrition and the second leading cause of death in children under the age of five, killing approximately 525,000 children each year.[3] Diarrhea is a symptom of numerous bacterial, parasitic, and viral infections that often result from the consumption of contaminated water.[3,5] The bacterial pathogen *Shigella* is a major contributor to diarrheal burden and is responsible for an estimated 90 million infections and 100,000 deaths annually, primarily occurring in the developing world where access to clean drinking water and appropriate medical care are limited.[8] However, the recent worldwide emergence of multidrug resistant *Shigella* strains[9,10] and the low dose necessary to initiate an infection (10–100 bacteria)[5] make *Shigella* a true worldwide health concern. Together, these factors underscore the need to fully understand the mechanism(s) *Shigella* employ to invade human host cells, evade host immune responses, and ultimately cause the symptoms associated with dysentery.[11–13] Like many Gram-negative bacterial pathogens, *Shigella* rely on *a* type three secretion system (T3SS) as a primary virulence factor.[14–17] The type three secretion apparatus (T3SA) is the heart of the system and resembles a nano-hypodermic needle and syringe that injects effector proteins directly from the bacterial cytoplasm into the host cell where they take over native function and support infection.[7,18–21] How the T3SA harnesses the energetics necessary to secrete effector proteins through the narrow (~2.5 nm diameter) channel of the apparatus has been of great interest,[22,23] but perhaps even more intriguing is the question of how protein secretion through the apparatus is regulated to minimize wasteful loss of effectors and maximize virulence.

T3SSs from bacterial pathogens including *Shigella*, *Yersinia*, *E. coli*, *Salmonella*, *Chlamydia*, and *Burkholderia* contain associated ATPases that are presumed to reside at the base of the apparatus and convert the potential energy in ATP to mechanical energy that supports protein unfolding and secretion through the apparatus.[24–29] Most recently, the *Shigella* protein Spa47 was identified as an oligomerization-dependent T3SS ATPase whose activity was directly linked to T3SA formation and protein secretion.[30] *Shigella* expressing Spa47 with mutations that eliminated ATP hydrolysis by either mutating active site residues or preventing Spa47 oligomer formation resulted in secretion-deficient strains that displayed wild-type growth characteristics in media, but were unable to infect cultured cells.[30]

Structural and biochemical analyses showed that Spa47 oligomerization is essential for completion of the active site(s) and ATPase activity.[24,30] Specifically, isolated/stable Spa47 oligomers exhibit significantly higher rates of ATP hydrolysis than isolated monomeric species. The Spa47 oligomers presumably contain pre-formed active sites at the protomer interfaces of the complex while Spa47 monomers must form transient activated multimers minimally consisting of two Spa47 molecules forming a single complete active site at the interface between the Spa47 protomers. The precise mechanistic role that T3SS ATP hydrolysis provides to support secretion, however, is unclear and somewhat controversial. The Spa47 homolog InvC from *Salmonella enterica* recognizes T3SS effector/chaperone complexes, releases the bound chaperone, and unfolds the effector proteins in an ATP-dependent manner, presumably preparing the effectors for secretion through the apparatus.[31] On the other hand, Erhardt et al. showed that a *S. enterica* strain expressing a catalytically inactive InvC mutant was secretion competent when an increased proton motive force (PMF) was generated across the inner bacterial membrane.[32] Similarly, protein secretion by the related flagellar type three secretion system was also shown to be independent of the ATPase FliI, but dependent on PMF.[32,33] Most recently, Morimoto and colleagues identified FliI as a critical component of a proton/protein antiporter in the flagellar T3SA, suggesting that ATP hydrolysis by FliI is not directly involved in protein unfolding and secretion.[34] Rather they suggest that PMF provides the energy required for the export gate to unfold proteins in preparation for secretion and that FliH supports efficient coupling of proton movement to protein secretion through the T3SA. Regardless of the specific mechanism(s) that T3SS ATPases employ, it seems clear that T3SS ATPases are critical for proper T3SA function and that they would make an ideal means of rapidly regulating T3SA activity *in vivo*, potentially activating secretion upon contact with host cells and downregulating activity to prevent wasteful protein secretion during times when the T3SS is not required.

Several examples of T3SS ATPase inhibition by protein interactions have been reported, supporting this hypothesis that T3SS activity is controlled via activity of the associated ATPase. Specifically, the *S. enterica* serovar Typhimurium flagellar protein FliH downregulated FliI activity *in vitro* by disrupting active FliI homo-hexamers and preventing ATP hydrolysis.[35] The FliI homologs YscL and CdsL from the *Y. enterocolitica* and *C. pneumoniae* T3SSs, respectively, also downregulated the activity of their respective ATPases *in vitro*[25,28] with overexpression of YscL in wild-type *Y. enterocolitica* decreasing protein secretion levels *in vivo*.[25] Fewer examples of T3SS ATPase activation are available, though oligomerization plays a clear role.[24,36–39] Additionally, FliI activity was shown to increase 10-fold in the presence of phospholipids[40] and 5-fold following exposure to an engineered FliH mutant lacking its 5 C-terminal residues,[41] suggesting that T3SS ATPase activity can be both up and downregulated in response to specific molecular interactions.

In this study, we investigated the interaction between the *Shigella* T3SS ATPase, Spa47 and the FliH homolog, MxiN. MxiN interaction with Spa47 was confirmed both *in vitro* and *in vivo*, identifying specific residues in Spa47 that are required for the interaction. A liposome flotation assay showed that MxiN interacts with phospholipid membranes and Spa47 simultaneously, perhaps providing a membrane anchor to help locate the highly-soluble Spa47 within the cytoplasmic T3SA sorting platform. Additionally, we found MxiN not only downregulates oligomeric Spa47 activity, but that it also upregulates the ATPase activity of

monomeric Spa47. Biochemical and biophysical analyses of MxiN and Spa47, characterization of MxiN/Spa47 interactions, and detailed kinetic analyses describe an unprecedented differential regulation of the T3SS ATPase Spa47 by a single T3SS protein and provide insight into the mechanism through which MxiN regulates Spa47 activity.

Experimental Procedures

Materials

Wild-type *S. flexneri* corresponds to the serotype 2a 2457T strain originally isolated in 1954.[42] The *S. flexneri spa47* null strain was engineered by Abdelmounaaïm Allaoui as described in Jouihri *et al*.[43] *E. coli* strains and 2X ligation mix were from Novagen (Madison, WI). Restriction enzymes, the pTYB21 protein expression plasmid, PCR buffer, Phusion High-Fidelity polymerase, and chitin resin were purchased from New England Biolabs (Ipswich, MA). Oligonucleotide primers and the synthesized *spa47* gene were from Integrated DNA Technologies (Coralville, IA). Defibrinated sheep blood was from Colorado Serum Company (Denver, CO) and HeLa cells were from the American Type Culture Collection (Manassas, VA). The Superdex 200 Increase 10/300 size exclusion, 5 mL HisTrap Crude FF, and 5 mL HiTrapQ FF columns were purchased from GE Healthcare (Pittsburgh, PA). ATP and asolectin were from Sigma–Aldrich (St. Louis, MO) and α-^{32}P-ATP was from Perkin Elmer (Boston, MA). Dithiothreitol (DTT), ampicillin, and chloramphenicol were from Gold Biotechnology (St. Louis, MO). Mouse anti-6x-Histidine primary antibodies were from Santa Cruz Biotechnology (Dallas, TX) and Alexa Fluor 647 goat anti-mouse secondary antibodies were purchased from Thermo Scientific (Rockford, IL). All other solutions and chemicals were of reagent grade.

Cloning

The *spa47* gene was purchased as a double-stranded gBlock product from Integrated DNA Technologies with modifications for cloning into the expression plasmid pTYB21 encoding an N-terminal chitin binding domain (CBD) and intein linker as described previously.[24] The Spa47$^{\Delta 1\text{-}6}$ and Spa47$^{\Delta 1\text{-}79}$ N-terminal truncations were generated in pTYB21 using inverse PCR and the *spa47*/pTYB21 construct as a template. The gene encoding MxiN was amplified from the *S. flexneri* 2457t strain and ligated into the expression plasmid pET15b. *mxiN* was similarly cloned into the first multiple cloning site of pACYCDuet-1. All constructs were sequence verified by Sanger sequencing (Genewiz, Inc., South Plainfield, NJ)

Protein expression and purification

E. coli Tuner (DE3) cells transformed with *mxiN* in pET15b were streaked onto a LB agarose plate containing 0.1 mg/mL ampicillin, incubated overnight at 37 C, and used to start fresh 1 L Terrific Broth (TB) cultures containing 0.1 mg/mL ampicillin. The cultures were grown to an OD_{600} of 0.8 at 37 C and 200 RPM (New Brunswick Innova 44) prior to inducing with 1 mM Isopropyl β-D-1-thiogalactopyranoside (IPTG) (20 h, 17 ° C, 200 RPM). The expressed MxiN was harvested by first separating the cells from the media by centrifugation followed by re-suspension in binding buffer (20 mM Tris, 500 mM NaCl, 5 mM imidazole, 5% (v/v) glycerol, pH 7.9) containing 0.2 mM of the protease inhibitor 4-(2-

aminoethyl) benzenesulfonyl fluoride hydrochloride (AEBSF) and membrane disruption by sonication. The suspension was clarified by centrifugation and the soluble MxiN was purified using an IMAC affinity column (5 mL GE HisTrap Crude FF) connected to an ÄKTA FPLC and eluted using a 0% to 100% elution buffer gradient (20 mM Tris, 500 mM NaCl, 400 mM imidazole, 5% (v/v) glycerol, pH 7.9) over 40 column volumes. IMAC elution fractions containing purified MxiN were assessed by SDS-PAGE and the peak fractions were buffer exchanged into 20 mM Tris 100 mM NaCl, 5 mM DTT, 5% (v/v) glycerol, pH 7.9 using PD 10 desalting columns (GE Healthcare). The buffer exchanged protein was then pooled and concentrated to approximately 30 μM using a Sartorius centrifugal concentrator with a 30 kDa molecular weight cut off. Concentration was determined using in gel densitometry of Coomassie stained acrylamide gels and bovine serum albumin as a standard.

spa47, *spa47*$^{\Delta 1\text{-}6}$, *and spa47*$^{\Delta 1\text{-}79}$ in pTYb21 were independently transformed into *E. coli* Tuner (DE3) cells and expressed as described previously for Spa47.[24] Following isolation from the media, the cells were re-suspended in 20 mM Tris, 500 mM NaCl, pH 7.9 containing 0.2 mM AEBSF and lysed by sonication. The Spa47 constructs were purified from the clarified supernatant using hand poured chitin resin columns (New England Biolabs, Ipswich, MA) to bind the N-terminal chitin binding domains of the expressed chimeras (10 mL resin / liter of culture). The Spa47 proteins were released from the resin by on-column intein cleavage with 50 mM DTT. Column elutions were collected over the course of several days until no further elution of Spa47 was observed by SDS-PAGE (~3 days). The elution fractions were diluted, resulting in a final buffer concentration of 20 mM Tris, 100 mM NaCl, 10 mM DTT, pH 7.9 prior to purification by negative selection over two tandem 5 mL Q Sepharose FF anion exchange columns. The purified Spa47 in the flow through was concentrated using a Sartorius centrifugal concentrator with a 30 kDa molecular weight cut off and further purified/characterized using a Superdex 200 Increase 10/300 size exclusion column equilibrated with 20 mM Tris, 100 mM NaCl, 5 mM DTT, pH 7.9. Spa47 concentrations were determined using in gel densitometry of Coomassie stained protein with bovine serum albumin as a standard. All Spa47 concentrations are reported in monomer concentration units for consistency and clarity.

Far-UV circular dichroism (CD)

Far-UV CD spectra and thermal stability profiles were obtained for purified monomeric and trimeric Spa47, Spa47$^{\Delta 1\text{-}6}$, Spa47$^{\Delta 1\text{-}79}$, and MixN. Measurements were collected using a JASCO model J-1500 spectropolarimeter equipped with a six-position sample holder and a Peltier temperature controller (Jasco, Easton, MD). Spectra were collected from 190 to 260 nm at 10 °C using 0.1 cm quartz cuvettes, 0.1 nm data sampling, a 50 nm/min scan rate, and a 2 second data integration time. Secondary structure thermal stability profiles were collected in the same 0.1 cm quartz cuvettes by monitoring the CD signal at 222 nm while the solution temperature was increased from 10 °C to 90 °C at a rate of 0.3 °C/min. CD analysis was performed on 0.5 mg/mL protein for MxiN, isolated monomeric Spa47, Spa47$^{\Delta 1\text{-}6}$, and Spa47$^{\Delta 1\text{-}79}$, and 0.3 mg/ml for isolated trimeric Spa47. MxiN was evaluated in 20 mM Tris, 100 mM NaCl, 5% (v/v) glycerol, 5 mM DTT, pH 7.9 and all Spa47 samples were in 20 mM Tris, 100 mM NaCl, and 5 mM DTT, pH 7.9. CD signals were converted to

mean residue molar ellipticity and secondary structure content analysis was performed using the Dichroweb[44] software package K2D.[45] Thermal unfolding transition temperatures (Tm) were determined by plotting the derivative of each thermal unfolding curve and identifying the corresponding maxima.

Analytical ultracentrifugation

Sedimentation velocity analytical ultracentrifugation (SV-AUC) experiments were conducted using an Optima XL-I (Beckman Coulter, Fullerton, CA) analytical ultracentrifuge equipped with scanning UV/visible optics. A 50 Ti eight-hole rotor and cells with Beckman 12 mm path length charcoal-epon two sector centerpieces and quartz windows were used. Protein samples were analyzed at 20 C and 40,000 RPM using absorbance detection at 280 nm and scanning until complete sedimentation was achieved. Scans were performed at multiple protein concentrations to ensure that the obtained results were concentration-independent (3.4 μM and 16.8 μM for MxiN; 10.7 μM and 18.5 μM for Spa47$^{\Delta 1\text{-}6}$). The data were analyzed using a continuous c(s) distribution and SEDFIT version 15.01b.[46] The buffer densities, buffer viscosities, and the protein partial specific volumes were calculated using Sednterp version 20130813 BETA.[47]

Phenotype characterization of Spa47 N-terminal truncation mutants

The impact of the Spa47$^{\Delta 1\text{-}6}$ and Spa47$^{\Delta 1\text{-}79}$ truncations on *Shigella* phenotype were evaluated using both a T3SS-medited red blood cell hemolysis assay[48] and a gentamicin protection (cellular invasion) assay.[49] The hemolysis assay measures the ability of *Shigella* to form a translocon pore in the membranes of red blood cells through proper translocator recruitment and T3SA maturation. Hemolytic activity was quantified by measuring hemoglobin release from red blood cells following incubation with *Shigella* expressing Spa47$^{\Delta 1\text{-}6}$ or Spa47$^{\Delta 1\text{-}79}$ and comparing to levels resulting from a strain expressing wild-type Spa47 (100% hemolysis). *Shigella* expressing Spa47$^{\Delta 1\text{-}6}$ and Spa47$^{\Delta 1\text{-}79}$ were also tested for their ability to invade cultured HeLa cells in a standard gentamycin protection assay using a *Shigella* strain expressing wild-type Spa47 as the positive control (100% invasion).

Liposome flotation assay

Asolectin, a natural soybean phospholipid mixture, was made to 8.7 mg/mL in the buffer corresponding to the protein(s) tested and was briefly sonicated using a probe sonicator. The lipid mixture was extruded at 50 °C using a 100 nm pore-sized membrane and an Avanti polar lipids extruder. Two micromolar MxiN was incubated with 4.4 mg/mL liposomes for 30 min at room temperature in 20 mM Tris, 100 mM NaCl, 5 mM DTT, pH 7.9. The mixture was brought up to 30% sucrose and 600 μL was transferred to an 11 x 60 mm ultracentrifugation tube and overlaid with 3 mL of 22.5% sucrose followed by 150 μL of buffer containing no sucrose. The samples were centrifuged in a Beckman SW-60 rotor using a Beckman XL-90 ultracentrifuge at 4 °C and 250,000 x g for 1 h 45 min. 100 μL aliquots were taken from the top, middle, and bottom regions of the sucrose gradient and analyzed for protein content by SDS-PAGE. This assay also monitored *in vitro* MxiN/Spa47 interactions by testing the ability of each Spa47 construct to “float” with liposomes in the presence and absence of MxiN. One micromolar Spa47 was prepared in the presence and

absence of 2 μM MxiN, incubated with 4.4 mg/mL asolectin liposomes, and analyzed as described above for MxiN alone.

ATP hydrolysis activity assay

Spa47 ATPase activity was measured using a radioactive α-^{32}P-ATP multiple time point activity assay as described previously.[24,30] Briefly, Spa47 was incubated for 30 minutes at room temperature in the tested condition and the reactions initiated by combining Spa47 with a prepared ATP solution resulting in a final concentration of 1 mM ATP, 10 mM $MgCl_2$, and 0.5 μCi (~300 nM) α-^{32}P-ATP. Samples were removed from the reaction at defined time points and rapidly quenched with a final concentration of 250 mM ethylenediaminetetraacetic acid (EDTA). The level of ATP hydrolysis at each time point was quantified separating the unreacted α-^{32}P-ATP substrate and the α-^{32}P-ADP product by TLC and detected with a Storm PhosphorImager (Molecular Dynamics). The concentration of ADP formed was quantified using ImageQuant software (Molecular Dynamics), and plotted as a function of reaction time to provide a rate of ATP hydrolysis for each enzyme under each condition tested.

Kinetic analysis of Spa47

K_M and V_{max} values were determined for full-length monomeric Spa47, full-length trimeric Spa47, and the monomeric Spa47$^{\Delta 1\text{-}6}$ construct. The assays were performed at 0.45, 0.225 and 1.35 μM enzyme concentrations for full-length monomeric and trimeric Spa47 and for the Spa47$^{\Delta 1\text{-}6}$ N-terminal truncation, respectively. Initial reaction velocities were determined for 0.025, 0.05, 0.1, 0.25, 0.5, and 1 mM ATP concentrations and plotted as initial velocity versus ATP concentration. SigmaPlot 12 was used to fit each dataset to the Michaelis-Menten equation:

$$v = \frac{V_{max}[S]}{K_M + [S]} \quad \text{(Equation 1)}$$

where v is the initial reaction velocity, [S] is the substrate concentration, K_M is the Michaelis constant, and V_{max} is the maximum velocity of the enzyme. Identical kinetic analyses were performed on full-length monomeric and trimeric Spa47 in the presence of saturating concentrations of MxiN (4.05 μM and 6.75 μM, respectively).

Spa47 regulation by MxiN

The effect of MxiN on the rate of ATP hydrolysis was examined for isolated full-length monomeric Spa47, isolated full-length trimeric Spa47, and the Spa47$^{\Delta 1\text{-}6}$ construct. The concentration of Spa47 monomer was held constant at 0.45 μM while exposed to increasing concentrations of MxiN (0, 0.225, 0.45, 0.9, 1.35, 1.8, 2.7, 4.05 and 5.4 μM) and the initial reaction rates determined as described above. This assay was repeated for the full-length Spa47 trimer, incubating 0.225 μM Spa47 with 0, 0.1125, 0.225, 0.45, 0.675, 0.9, 1.35, 2.025, 2.7, 4.5, and 6.75 μM MxiN. Spa47$^{\Delta 1\text{-}6}$ was tested at 1.35 μM Spa47$^{\Delta 1\text{-}6}$ in the presence of 0, 1.35, 2.7, 4.5 and 6.75 μM MixN. Bovine serum albumin (BSA) was substituted for MxiN as a negative control.

Spa47/MxiN co-expression and co-purification

spa47, *spa47*$^{\Delta 1\text{-}6}$, and *spa47*$^{\Delta 1\text{-}79}$ in pTYB21 were independently co-transformed into *E. coli* Tuner (DE3) cells with *mxiN* in MCS1 of pACYCDuet-1 and purified following the protocol for Spa47 purification described above, with the exception that both ampicillin and chloramphenicol were included in the growth media to maintain the expression plasmids. Spa47 and any bound MxiN was purified from the soluble cell lysate using chitin resin exactly as was done for Spa47 alone. The elution fractions were evaluated by SDS-PAGE and western blot analysis probing for the 6X-Histidine tag on MxiN. The full-length Spa47/MxiN complex was further purified via anion exchange column and evaluated using an ÄKTA purifier equipped with a Superdex 200 Increase 10/300 size exclusion column, UV detection, and fraction collecting capabilities. The fractions were visualized by SDS-PAGE to identify the protein contents of each peak in the chromatogram.

Results

Insights from the flagellar secretion system

A recent 2.4 Å crystal structure of Spa47 found that it is structurally similar to the flagellar ATPase FliI with an average pairwise root-mean-square deviation (RMSD) for Cα atoms between Spa47 (PDB ID 5SWJ) and FliI (PDB ID 2DPY) of 1.43 Å over 310 atoms, supported by a 37% sequence identity between the two enzymes.[30,50] From this and our previous findings that Spa47 is an oligomerization-dependent ATPase,[24,30] we hypothesized that the enzymatic activity of translocon-associated T3SS ATPases such as Spa47 may be regulated by specific protein interactions, as seen in the flagellar system where activity of the ATPase FliI is reduced upon binding FliH.[35] Comparison of cryo-electron tomography structures of the *Helicobacter* flagellar secretion apparatus[6] to the basal body and sorting platform of the *Shigella* T3SS[7] clearly highlights the structural similarities and differences between the complexes (Figure 1). For example, the ATPases FliI and Spa47 are similarly located at the bottom of the flagellar and *Shigella* T3SS basal body structures, respectively; located just below the entrance to the apparatus export channels and colored red for contrast (Figure 1). The ATPase regulator FliH is colored yellow in the flagellar structure with six copies extending radially out from the oligomeric FliI ring. Comparison to the *Shigella* T3SA basal body shows that six similar extensions of electron density radiate from the Spa47 structure (Figure 1B). This density has previously been assigned to MxiN, a predicted homolog of FliH.[7] These marked similarities within the cryo-electron tomography structures suggest that MxiN may be a functional homolog of FliI and provide a regulatory role for Spa47 similar to that seen between FliI and FliH. Comparison of the MxiN and FliH sequences identifies an 18% sequence identity and predicted secondary structures that modestly align with one another (Figure 1C). Multiple sequence alignment of MxiN and 8 predicted homologs from other T3SSs shows that the sequence identity among individuals within the group ranges from 7.95% to 55.24% identity to one another (Figure S1).

Biophysical characterization of MxiN and the Spa47 N-terminal-deletion constructs, Spa47$^{\Delta 1\text{-}79}$ and Spa47$^{\Delta 1\text{-}6}$

To test the hypothesis that MxiN influences Spa47 activity, we recombinantly expressed and purified MxiN, oligomeric and monomeric full-length Spa47, the exclusively monomeric

Spa47$^{\Delta 1\text{-}79}$ construct crystallized previously, and a newly engineered Spa47$^{\Delta 1\text{-}6}$ construct we hypothesized to also purify as an exclusive monomer. Each of the proteins were analyzed by far-UV circular dichroism and the previously untested MxiN and Spa47$^{\Delta 1\text{-}6}$ constructs were characterized by analytical ultracentrifugation to better understand the physical properties of MxiN and the effects of the Spa47 N-terminal deletion on the overall protein structure and oligomerization properties. The far-UV CD spectra of isolated monomeric Spa47, Spa47$^{\Delta 1\text{-}6}$, and Spa47$^{\Delta 1\text{-}79}$ overlay on one another with the isolated Spa47 oligomer exhibiting a slightly attenuated CD signal (Figure 2A). Analysis of the CD spectra show that isolated monomeric Spa47 and the Spa47$^{\Delta 1\text{-}6}$ truncation share nearly identical secondary structure content ratios while the Spa47$^{\Delta 1\text{-}79}$ construct results in an increase in α-helix content and a decrease in random coil (Table 1). Spa47 oligomerization decreases the α-helix content and increases the percentage of random coil compared to any of the monomeric constructs. CD thermal unfolding curves were collected for each of the Spa47 constructs with sharp transitions observed at 42.8 ± 0.2 °C, 45.3 ± 0.2 °C and 47.8 ± 0.4 °C, for full-length monomeric Spa47, Spa47$^{\Delta 1\text{-}6}$, and Spa47$^{\Delta 1\text{-}79}$, respectively (Figure 2B and Table 1). As seen previously, the thermal transition of trimeric Spa47 is significantly shallower than observed for monomeric Spa47,[24] with a transition temperature of 40.2 ± 0.7 °C. The far-UV CD spectrum of MxiN exhibits well-defined minima at 208 nm and 222 nm, consistent with a highly α-helical secondary structure (Figure 2C). Spectral analysis identified MxiN as 59 ± 0.1% α-helix, 8 ± 0.1% β-strand, and 33 ± 0.0% random coil (Table 1). The thermal unfolding profile for MxiN contains a sharp transition at 35.6 ± 0.3 °C (Figure 2D), suggesting that recombinant MxiN is susceptible to moderate thermal stress.

We additionally observed that purified MxiN precipitated when analyzed by gel filtration chromatography, but that it was amendable to analysis by analytical ultracentrifugation (AUC), finding that MxiN sediments nearly exclusively as a single species with a sedimentation coefficient of 2.34 Svedbergs, consistent with a stable MxiN homo-dimer in solution (Figure S2). The Spa47$^{\Delta 1\text{-}6}$ protein lacking the six N-terminal residues of Spa47 was also analyzed by AUC, identifying a predominantly monomeric species with a sedimentation coefficient of 2.97 Svedbergs, consistent with previous reports for Spa47$^{\Delta 1\text{-}79}$ and findings that deletion of the seven N-terminal residues from FliI prevented ATP-dependent hexamer formation.[30,51] Notably, however, the Spa47$^{\Delta 1\text{-}6}$ mutant does exhibit a very minor population of oligomeric species with a sedimentation coefficient of approximately 5.5 Svedbergs, consistent with that of the ATPase active homo-trimeric complex identified for full-length Spa47,[24] though the Spa47$^{\Delta 1\text{-}6}$ oligomer was unable to be isolated due to such low abundance. Together, these findings suggest that the targeted six N-terminal residues in Spa47 are necessary for proper oligomer formation, though their absence does not entirely preclude oligomerization (Figure S2), providing a valuable construct for probing the effects of oligomer formation on Spa47 kinetics.

Spa47 N-terminus is required for efficient ATPase activity

The ability of the primarily monomeric Spa47$^{\Delta 1\text{-}6}$ construct to hydrolyze ATP was examined under substrate-saturating conditions and compared to isolated monomeric and trimeric full-length Spa47 and the Spa47$^{\Delta 1\text{-}79}$ truncation mutation (Figure 3A). As shown previously, the

Spa47 trimer provided a significantly higher rate of ATP hydrolysis than the isolated monomer (0.85 ± 0.03 μmol ADP min^{-1} mg $Spa47^{-1}$ and 0.24 ± 0.01 μmol ADP min^{-1} mg $Spa47^{-1}$, respectively) while the $Spa47^{\Delta 1-79}$ construct was completely inactive.[30] Unexpectedly, the $Spa47^{\Delta 1-6}$ construct engineered in this study demonstrated a significantly reduced, yet robust rate of hydrolysis of 0.11 ± 0.01 μmol ADP min^{-1} mg $Spa47^{-1}$, intermediate to the rates of the isolated full-length monomer and the inactive $Spa47^{\Delta 1-79}$ mutant.

The effect of substrate concentration on the kinetics of each of the active full-length Spa47 species was tested (Figure 3B). Each demonstrated substrate-dependent rates that were fit to the Michaelis-Menten equation (Equation 1) and used to determine K_M, V_{max}, k_{cat}, and k_{cat}/K_M for each Spa47 species (Table 2). The K_M for the isolated trimer was 114 ± 20 μM, the isolated monomer was 181 ± 30 μM, and the K_M for $Spa47^{\Delta 1-6}$ was 269 ± 31 μM. As expected, the V_{max} and k_{cat} determined for each of the constructs tracked well with the trend in rates observed from Figure 3A, decreasing from Spa47 trimer to Spa47 monomer to $Spa47^{\Delta 1-6}$. The k_{cat}/K_M values for Spa47 trimer, Spa47 monomer, and $Spa47^{\Delta 1-6}$ were 7.5 ± 1.2 x 10^3 M^{-1} sec^{-1}, 1.3 ± 0.2 x 10^3 M^{-1} sec^{-1}, and 4.2 ± 0.3 x 10^2 M^{-1} sec^{-1}, respectively.

The effect of the $Spa47^{\Delta 1-6}$ and $Spa47^{\Delta 1-79}$ truncations on *Shigella* phenotype were tested using red blood cell hemolysis and gentamycin protection (cellular invasion) assays. Consistent with our previous findings, complementing a Spa47 knockout *Shigella* strain with the ATPase inactive $Spa47^{\Delta 1-79}$ construct eliminated both hemolytic and invasion phenotypes (Table3).[30] The $Spa47^{\Delta 1-6}$ complemented strain exhibited wild-type hemolysis and invasion phenotypes at 100 ± 6% and 89 ± 19%, respectively, suggesting that perhaps additional protein interactions within the context of the *Shigella* T3SS overcome the oligomerization and ATPase deficiencies of $Spa47^{\Delta 1-6}$ observed *in vitro*.

MxiN interacts through the extreme N-terminus of Spa47

An *in vitro* liposome flotation assay was developed to specifically probe the ability of MxiN to interact with the various isolated oligomer states and engineered N-terminal truncation constructs of Spa47. We first demonstrated that MxiN interacts with liposomes and “floats” to the top layer of a discontinuous sucrose gradient when incubated with liposomes and centrifuged (Figure 4). MxiN interaction with the liposomes appears to be peripheral as the presence of a moderate NaCl concentration (500 mM) disrupts the interaction between MxiN and the liposomes and results in MxiN remaining in the bottom fraction of the sucrose gradient following centrifugation. Isolated recombinant full-length Spa47 monomer and trimer were similarly tested and found to not interact with liposomes in this assay; monomeric and trimeric Spa47 remained in the bottom fraction of the sucrose gradient following incubation with liposomes and centrifugation. The inability of Spa47 to directly interact with phospholipid membranes was unexpected as the related ATPases FliI,[40] InvC,[27] and HrcN[37] from the *Salmonella* flagellar motor, *Salmonella* T3SS, and *Pseudomonas* T3SS, respectively, all interact with phospholipid membranes *in vitro*. Interestingly, however, the Spa47 monomer and trimer species both efficiently “floated” to the top of the sucrose gradient when incubated with a combination of MxiN and liposomes. This indicates

that both Spa47 species "floated" through direct interaction with MxiN, which was itself interacting with the liposomes and that the interaction is insensitive to Spa47 oligomer state. The interaction was, however, entirely dependent on the N-terminus of Spa47 as neither Spa47$^{\Delta 1\text{-}79}$ nor Spa47$^{\Delta 1\text{-}6}$ "floated" in the absence or presence of MxiN (Figure 4), consistent with studies showing that the N-terminus of the flagellar ATPase FliI is required for interaction with its inhibitor FliH.[52] Together, these findings have identified the six N-terminal residues in Spa47 as critical for proper MxiN/Spa47 interaction *in vitro* and have provided a much-needed Spa47 control for the following experiments testing the effect of MxiN on Spa47 activity.

MxiN differentially regulates the activity of monomeric and oligomeric Spa47

The effect of MxiN on Spa47 ATPase activity was tested for full-length monomeric and trimeric Spa47 and for Spa47$^{\Delta 1\text{-}6}$. When trimeric Spa47 activity was tested with increasing concentrations of MxiN, the activity decreased exponentially from 0.88 sec^{-1} to 0.42 sec^{-1}, saturating with the addition of ~3 μM MxiN (Figure 5A). Surprisingly, however, when the effect of MxiN on Spa47 monomer was tested, an opposite effect was observed. The k_{cat} of the monomer increased from approximately 0.25 sec^{-1} in the absence of MxiN to over 0.49 sec^{-1} at MxiN concentrations greater than 4 μM (Figure 5A). The activity of the Spa47$^{\Delta 1\text{-}6}$ construct was just over 0.1 sec^{-1} and was unaffected by the addition of MxiN, consistent with our findings that Spa47$^{\Delta 1\text{-}6}$ is unable to bind MxiN *in vitro* (Figure 4). The effect of BSA on the activity of each Spa47 construct was tested, confirming that the effect of MxiN on Spa47 activity is specific and not the result of molecular crowding or non-specific protein interactions (Figure S3).

Substrate-dependent kinetic analyses of isolated monomeric and trimeric Spa47 in the presence and absence of saturating concentrations of MxiN were performed (Figure 5B). The kinetic parameters K_M, V_{max}, k_{cat}, and k_{cat}/K_M were determined for each condition by fitting the data to the Michaelis-Menten equation (Equation 1). As expected from the results in Figure 5A, V_{max} for the Spa47 trimer reduced from 1.04 ± 0.02 μmol ADP min^{-1} mg Spa47^{-1} to 0.62 ± 0.06 μmol ADP min^{-1} mg Spa47^{-1} and V_{max} for the monomer increased from 0.28 ± 0.01 μmol ADP min^{-1} mg Spa47^{-1} to 0.51 ± 0.01 μmol ADP min^{-1} mg Spa47^{-1} in the presence of MxiN (Table 2). The k_{cat} values followed identical trends since the total enzyme concentration was not changed with increasing concentrations of MxiN. While the K_M of the trimeric Spa47 (114 ± 20 μM) is noticeably lower than the apparent K_M of monomeric Spa47 (181 ± 30 μM), the addition of MxiN did not alter the observed K_M values for either the trimeric or monomeric forms of Spa47, remaining at 116 ± 19 μM and 201 ± 8 μM, respectively. The changes in V_{max} following addition of MxiN, however, differentially influenced the overall enzyme efficiency of the Spa47 trimer and monomer. The k_{cat}/K_M of the Spa47 oligomer decreased from 7.5 ± 1.2 x 10^3 M^{-1} sec^{-1} to 4.4 ± 0.3 x 10^3 M^{-1} sec^{-1} following addition of MxiN. The k_{cat}/K_M of the monomeric Spa47 was 1.3 ± 0.2 x 10^3 M^{-1} sec^{-1} and 2.1 ± 0.1 x 10^3 M^{-1} sec^{-1} in the absence and presence of MxiN, respectively.

MxiN interacts with Spa47 in vivo

Tagless MxiN and the previously engineered CBD-intein-Spa47 chimera[24,30] were co-expressed in *E. coli* and co-purified via chitin resin, on-column cleavage of the intein domain, anion exchange chromatography, and size exclusion chromatography. The resulting size exclusion chromatogram and associated SDS-PAGE gel clearly show that MxiN interacts with Spa47 and that the Spa47/MxiN hetero-oligomeric complex elutes from the sizing column with a retention volume between those of isolated monomeric and trimeric Spa47 (Figure 6). Co-expression of MxiN with either of the engineered N-terminal truncation mutants ($Spa47^{\Delta 1\text{-}79}$ and $Spa47^{\Delta 1\text{-}6}$) resulted in little-to-no MxiN observed in the chitin elution fractions (Figure S4), consistent with the *in vitro* liposome flotation assay showing that MxiN interacts through the N-terminal domain of Spa47. In-gel densitometry analysis of the isolated Spa47/MxiN complex identified a 2:1 MxiN:Spa47 stoichiometry, in agreement with the SEC retention volume that more specifically suggests the isolated complex is a $MxiN_2Spa47$ hetero-trimer (Figure 6) with no higher molecular weight/stoichiometry MxiN/Spa47 complexes observed. Substrate-dependent ATPase activity of the co-expressed and co-purified $MxiN_2Spa47$ verified that the co- purified complex is in fact active with a K_M of 208 ± 19 μm and a V_{max} of 0.28 ± .01 μmol min^{-1} mg $Spa47^{-1}$ (Figure S5). When compared to the MxiN/Spa47 species formed by titrating purified Spa47 with MxiN (Table 2), the K_M of the co-purified species is nearly identical to that of the Spa47/MxiN complex derived from isolated Spa47 monomer while the V_{max} is lower and equal to that of the isolated Spa47 monomer in the absence of MxiN.

Discussion

T3SSs are complex nano-machines capable of injecting effector proteins directly into the host cell cytoplasm.[17,53] Like many pathogens expressing T3SSs, *Shigella* rely on these injected effectors to promote pathogen uptake by the host cell and to help circumvent host immune responses.[14,15] This reliance on T3SSs for infection together with the rapid emergence of antibiotic resistant bacteria makes T3SSs ideal targets for anti-infective therapeutics and underscores the importance of understanding the mechanism(s) that activate and regulate protein secretion through the T3SA. Regulation of the *Shigella* T3SS begins with tight control over transcription of the genes encoding structural T3SA components and secreted effector proteins, supporting transcription at temperatures approaching 37 °C.[54,55] Once the T3SA components are expressed and the apparatus is assembled, it serves as an environmental sensor of small molecules such as bile salts, sphingolipids, and cholesterol, promoting a discrete stepwise maturation of the *Shigella* T3SA tip complex that prepares the apparatus for fusion with a host cell membrane.[56-60] Despite a strong understanding of the environmental stimuli driving maturation and activation of the *Shigella* T3SA, the means through which T3SA activation and protein secretion is achieved remains largely unclear. Uncovering the link between Spa47 ATPase activity, T3SA formation, secretion of T3SS effector proteins, and *Shigella* virulence[30], however, suggests that control over T3SS ATPase activity would provide a powerful means for *Shigella* to rapidly up and downregulate activity of the T3SA.

The ability to purify active monomeric and oligomeric populations of Spa47 has been instrumental in describing the role of Spa47 oligomerization in *Shigella* T3SS function.[24,30] For example, the increased ATP hydrolysis rates seen for trimeric Spa47 compared to the monomeric Spa47 appear to result from pre-formed active sites in the Spa47 oligomer that include critical sidechain contributions from adjacent Spa47 protomers.[30] Activity in the monomeric population, however, requires not only binding ATP, but also a transient interaction with one or more Spa47 monomers to complete the functional P-loop active site and support hydrolysis, perhaps similar to the conditions seen within the *Shigella* cytoplasm. Extending these studies has allowed us to more directly investigate the role of T3SS ATPases in virulence regulation by characterizing monomeric and oligomeric Spa47 species with respect to enzyme kinetics, MxiN interaction, and ultimately ATPase regulation.

In kinetic studies, we showed that Spa47 monomer is overall less efficient than the trimer, exhibiting both a higher apparent K_M and a lower apparent V_{max}. Interestingly, the Spa47$^{\Delta 1\text{-}6}$ construct has an even lower apparent V_{max} than the isolated full-length monomeric species though they share similar substrate sensitivities (K_M). The trending decrease in V_{max} when comparing Spa47 trimer to monomer to Spa47$^{\Delta 1\text{-}6}$ is consistent with a decrease in the number of "activated" species available in solution when comparing Spa47 oligomers to monomers. It is also interesting that the K_M of the oligomer is lower than those of both the full-length monomer and Spa47$^{\Delta 1\text{-}6}$. It is important to recognize, however, that the kinetic parameters identified for the isolated monomeric Spa47 species (Spa47 monomer and Spa47$^{\Delta 1\text{-}6}$) are heavily influenced by the ability of the monomers to form transient activated complexes that would minimally consist of dimeric Spa47 forming a single complete active site at the interface between the two protomers. The fact that full-length Spa47 monomer and Spa47$^{\Delta 1\text{-}6}$ have similar K_Ms (both higher than the trimer) despite a two-fold difference in V_{max} suggests that perhaps the pre-formed Spa47 oligomer exhibits a higher affinity for substrate than either of the monomeric forms and that the rate seen for Spa47$^{\Delta 1\text{-}6}$ is due to a decreased ability to form transient active species in solution. Further biophysical characterization and stoichiometric determination of the active Spa47 species resulting from each isolated population will be required to fully understand the influence of transient oligomerization on the reported monomeric Spa47 kinetic parameters, however, the overall effect of Spa47 oligomerization and MxiN interaction are clear, providing the means to both up and downregulate activity of the *Shigella* T3SA.

Similarities observed between the structural organization of the flagellar export apparatus and the *Shigella* T3SA sorting platform, together with previous findings that MxiN and Spa47 interact *in vivo*, led us to further characterize recombinant MxiN.[43,61] We show that recombinant MxiN is a highly α-helical homodimer in solution, in agreement with similar findings for the flagellar ATPase inhibitor, FliH.[62] Furthermore, we reveal that the interaction between MxiN and Spa47 is mediated by the N-terminus of the latter, and in particular, the first 6 residues, which are also critical for stable Spa47 oligomerization and activation *in vitro*. We therefore propose that MxiN directly influences Spa47 oligomerization and in turn influencing Spa47 activity. This notion is reinforced by SEC analyses that confirm the lack of Spa47 oligomers when Spa47 is co-expressed or co-purified with MxiN, and by the decreased activity of Spa47 observed in the presence of MxiN. Similar negative regulation of FliI by FliH (*Salmonella*),[35] YscN by YscL (*Yersinia*),

[25] and CdsN by CdsL (*Chlamydia*)[28] suggest that there is at least some level of functional conservation as T3SS ATPase repressors among the putative MxiN homologs.

In contrast, MxiN enhances the ATPase activity of monomeric Spa47, suggesting that MxiN differentially regulates Spa47 activity, depending on its initial oligomeric state. Insights from related systems suggest that MxiN may be involved in supporting the dynamic exchange of Spa47 between the T3SA basal body and the cytoplasm and/or perhaps in supporting distinct roles of Spa47 within the context of the T3SA. Specifically, Bai et al. showed that FliI is in dynamic exchange between the flagellar basal body and the bacterial cytoplasm and that 7 ± 3 copies of FliI were associated with each flagellar motor despite only six copies of FliI identified in cryo-electron tomography images.[63] Additional fluorescence and biochemical experiments suggested that while six copies of FliI form the homo-hexameric ATPase ring within the flagellar motor, the excess FliI proteins located at the basal body come from $FliH_2FliI$ complexes transiently interacting with the C-ring to deliver protein substrates for export through the apparatus. More recently, studies in *Yersinia enterocolitica* also found that many of the soluble sorting platform proteins (including the ATPase YscN and the negative regulator YscL) are in dynamic exchange between the T3SA and the bacterial cytoplasm and that again greater than the expected six copies of the ATPase were associated with the T3SA.[64] Together with the work presented here, these findings paint a picture of a dynamic apparatus that relies on the associated T3SS ATPase and regulator for multiple roles in supporting secretion and as a part of a signaling cascade responding to external stimuli. With respect to *Shigella*, one can imagine that MxiN association with Spa47 monomers in the cytoplasm may increase the propensity of Spa47 to form transient oligomers, resulting in the observed increase in ATPase activity. The resulting $MxiN_2Spa47$ complex may then serve as a proto-oligomer readied for incorporation into the T3SA and/or perhaps serve a similar function as $FliH_2FliI$ in introducing cytoplasmic substrate to the flagellar export apparatus for secretion. The inhibitory role of MxiN on oligomeric Spa47, on the other hand, may be required to reduce the activity of Spa47 oligomers that either form within the cytoplasm or result from dynamic exchange between the T3SA and cytoplasm, minimizing wasteful ATP hydrolysis by cytoplasmic Spa47 oligomers. Clearly, the findings presented here only begin to uncover the role of MxiN in the *Shigella* T3SS, but have provided a strong platform for comparing apparatus activation and regulation across multiple pathogens and supported a detailed kinetic analysis of Spa47 regulation by MxiN.

Our analyses find that Spa47 kinetics are altered upon MxiN binding, depending on Spa47 oligomeric state. Although V_{max} values for both Spa47 oligomeric species converge in the presence of MxiN, they are statistically different from one another, suggesting that the resulting complexes remain unique. Perhaps even more telling is the effect (or lack thereof) on the K_M of both Spa47 monomer and trimer following MxiN interaction; with the complex originating from Spa47 oligomer maintaining a lower K_M than that resulting from monomeric Spa47 despite significant/differential influences on V_{max}. It is additionally interesting to consider that while the $MxiN_2Spa47$ heterotrimer co-purified from *E. coli* exhibits a K_M consistent with isolated Spa47 monomer under saturating MxiN conditions, the V_{max} of the co-purified complex is significantly lower than expected from the *in vitro* mixing studies. The details surrounding this difference in the V_{max} values is not entirely clear, but perhaps the Spa47/MxiN interactions supported during co-expression are a better

mimic for those that take place in the *Shigella* cytoplasm directly following protein expression, resulting in a high K_M and low V_{max} to minimize wasteful ATP hydrolysis by cytoplasmic stores of Spa47. Regardless, the differential kinetic effects observed here suggest that interaction of MxiN with monomeric and oligomeric Spa47 results in distinct complexes with unique kinetic parameters that may play individually important roles in *Shigella* T3SA regulation. Moreover, it remains to be seen whether the differential regulation described here for Spa47 is unique to *Shigella*, or is shared among many or all T3SSs and has only now been observed because of the ability to isolate stable monomeric and oligomeric Spa47 species.

Supplementary Material

Refer to Web version on PubMed Central for supplementary material.

Acknowledgments

We thank the Dickenson lab members Abram Bernard and Jamie Burgess for scientific discussions and critical reading of the manuscript.

Funding Source Statement: This work was supported in part by a National Institutes of Health Grant 1R15AI124108-01A1, a National Science Foundation MRI Grant 1530862, and R. Gaurth Hansen endowment funds to N. E. D.

Abbreviations

AEBSF	4-(2-aminoethyl) benzenesulfonyl fluoride hydrochloride
BSA	bovine serum albumin
CBD	chitin binding domain
CD	circular dichroism
DTT	dithiothreitol
EDTA	ethylenediaminetetraacetic acid
PMF	proton motive force
IMAC	immobilized metal affinity chromatography
IPTG	Isopropyl β-D-1-thiogalactopyranoside
LB	Luria-Bertani
LPS	lipopolysaccharide
MCS	multiple cloning site
PDVF	polyvinylidene fluoride
PBS	phosphate buffered saline
RMSD	root-mean-square deviation

sv-AUC	sedimentation velocity analytical ultracentrifugation
T3SA	type three secretion apparatus
T3SS	type three secretion system
TB	terrific broth
TLC	thin layer chromatography
TSB	tryptic soy broth

References

1. The PyMOL Molecular Graphics System, version 1.8. Schrödinger, LLC;
2. McGuffin LJ, Bryson K, Jones DT. The PSIPRED protein structure prediction server. Bioinformatics. 2000; 16:404–405. [PubMed: 10869041]
3. World Health Organization. Diarrhoeal disease. (Updated May 2017). http://www.who.int/mediacentre/factsheets/fs330/en/
4. Pettersen EF, Goddard TD, Huang CC, Couch GS, Greenblatt DM, Meng EC, Ferrin TE. UCSF Chimera--a visualization system for exploratory research and analysis. J Comput Chem. 2004; 25:1605–1612. [PubMed: 15264254]
5. DuPont HL, Levine MM, Hornick RB, Formal SB. Inoculum size in shigellosis and implications for expected mode of transmission. J Infect Dis. 1989; 159:1126–1128. [PubMed: 2656880]
6. Qin Z, Lin WT, Zhu S, Franco AT, Liu J. Imaging the motility and chemotaxis machineries in Helicobacter pylori by cryo-electron tomography. J Bacteriol. 2016; 199:e00695–00616.
7. Hu B, Morado DR, Margolin W, Rohde JR, Arizmendi O, Picking WL, Picking WD, Liu J. Visualization of the type III secretion sorting platform of Shigella flexneri. Proc Natl Acad Sci U S A. 2015; 112:1047–1052. [PubMed: 25583506]
8. Kotloff KL. The Burden and Etiology of Diarrheal Illness in Developing Countries. Pediatr Clin North Am. 2017; 64:799–814. [PubMed: 28734511]
9. Dutta S, Ghosh A, Ghosh K, Dutta D, Bhattacharya SK, Nair GB, Yoshida S. Newly emerged multiple-antibiotic-resistant *Shigella dysenteriae* type 1 strains in and around Kolkata, India, are clonal. J Clin Microbiol. 2003; 41:5833–5834. [PubMed: 14662996]
10. Puzari M, Sharma M, Chetia P. Emergence of antibiotic resistant Shigella species: A matter of concern. J Infect Public Health. 2017; In Press. doi: 10.1016/j.jiph.2017.1009.1025
11. Killackey SA, Sorbara MT, Girardin SE. Cellular Aspects of Shigella Pathogenesis: Focus on the Manipulation of Host Cell Processes. Front Cell Infect Microbiol. 2016; 6:38. [PubMed: 27066460]
12. Agaisse H. Molecular and Cellular Mechanisms of Shigella flexneri Dissemination. Front Cell Infect Microbiol. 2016; 6:29. [PubMed: 27014639]
13. Yang SC, Hung CF, Aljuffali IA, Fang JY. The roles of the virulence factor IpaB in Shigella spp. in the escape from immune cells and invasion of epithelial cells. Microbiol Res. 2015; 181:43–51. [PubMed: 26640051]
14. Carayol N, Tran Van Nhieu G. The inside story of Shigella invasion of intestinal epithelial cells. Cold Spring Harb Perspect Med. 2013; 3:a016717. [PubMed: 24086068]
15. Phalipon A, Sansonetti PJ. Shigella's ways of manipulating the host intestinal innate and adaptive immune system: a tool box for survival? Immunol Cell Biol. 2007; 85:119–129. [PubMed: 17213832]
16. Puhar A, Sansonetti PJ. Type III secretion system. Curr Biol. 2014; 24:R784–791. [PubMed: 25202865]
17. Schroeder GN, Hilbi H. Molecular pathogenesis of *Shigella* spp.: controlling host cell signaling, invasion, and death by type III secretion. Clinical microbiology reviews. 2008; 21:134–156. [PubMed: 18202440]

18. Chatterjee S, Chaudhury S, McShan AC, Kaur K, De Guzman RN. Structure and biophysics of type III secretion in bacteria. Biochemistry. 2013; 52:2508–2517. [PubMed: 23521714]
19. Ashida H, Mimuro H, Sasakawa C. Shigella manipulates host immune responses by delivering effector proteins with specific roles. Front Immunol. 2015; 6:219. [PubMed: 25999954]
20. Schroeder GN, Jann NJ, Hilbi H. Intracellular type III secretion by cytoplasmic Shigella flexneri promotes caspase-1-dependent macrophage cell death. Microbiology. 2007; 153:2862–2876. [PubMed: 17768231]
21. Enninga J, Mounier J, Sansonetti P, Tran Van Nhieu G. Secretion of type III effectors into host cells in real time. Nat Methods. 2005; 2:959–965. [PubMed: 16299482]
22. Cordes FS, Komoriya K, Larquet E, Yang S, Egelman EH, Blocker A, Lea SM. Helical structure of the needle of the type III secretion system of Shigella flexneri. J Biol Chem. 2003; 278:17103–17107. [PubMed: 12571230]
23. Fujii T, Cheung M, Blanco A, Kato T, Blocker AJ, Namba K. Structure of a type III secretion needle at 7-A resolution provides insights into its assembly and signaling mechanisms. Proc Natl Acad Sci U S A. 2012; 109:4461–4466. [PubMed: 22388746]
24. Burgess JL, Jones HB, Kumar P, Toth RTt, Middaugh CR, Antony E, Dickenson NE. Spa47 is an oligomerization-activated type three secretion system (T3SS) ATPase from Shigella flexneri. Protein Sci. 2016; 25:1037–1048. [PubMed: 26947936]
25. Blaylock B, Riordan KE, Missiakas DM, Schneewind O. Characterization of the Yersinia enterocolitica type III secretion ATPase YscN and its regulator, YscL. J Bacteriol. 2006; 188:3525–3534. [PubMed: 16672607]
26. Andrade A, Pardo JP, Espinosa N, Perez-Hernandez G, Gonzalez-Pedrajo B. Enzymatic characterization of the enteropathogenic Escherichia coli type III secretion ATPase EscN. Arch Biochem Biophys. 2007; 468:121–127. [PubMed: 17964526]
27. Akeda Y, Galan JE. Genetic analysis of the Salmonella enterica type III secretion-associated ATPase InvC defines discrete functional domains. J Bacteriol. 2004; 186:2402–2412. [PubMed: 15060043]
28. Stone CB, Johnson DL, Bulir DC, Gilchrist JD, Mahony JB. Characterization of the putative type III secretion ATPase CdsN (Cpn0707) of Chlamydophila pneumoniae. J Bacteriol. 2008; 190:6580–6588. [PubMed: 18708502]
29. Gong L, Lai SC, Treerat P, Prescott M, Adler B, Boyce JD, Devenish RJ. Burkholderia pseudomallei type III secretion system cluster 3 ATPase BsaS, a chemotherapeutic target for small-molecule ATPase inhibitors. Infect Immun. 2015; 83:1276–1285. [PubMed: 25605762]
30. Burgess JL, Burgess RA, Morales Y, Bouvang JM, Johnson SJ, Dickenson NE. Structural and Biochemical Characterization of Spa47 Provides Mechanistic Insight into Type III Secretion System ATPase Activation and Shigella Virulence Regulation. J Biol Chem. 2016; 291:25837–25852. [PubMed: 27770024]
31. Akeda Y, Galan JE. Chaperone release and unfolding of substrates in type III secretion. Nature. 2005; 437:911–915. [PubMed: 16208377]
32. Erhardt M, Mertens ME, Fabiani FD, Hughes KT. ATPase-independent type-III protein secretion in Salmonella enterica. PLoS Genet. 2014; 10:e1004800. [PubMed: 25393010]
33. Minamino T, Namba K. Distinct roles of the FliI ATPase and proton motive force in bacterial flagellar protein export. Nature. 2008; 451:485–488. [PubMed: 18216858]
34. Morimoto YV, Kami-Ike N, Miyata T, Kawamoto A, Kato T, Namba K, Minamino T. High-Resolution pH Imaging of Living Bacterial Cells To Detect Local pH Differences. MBio. 2016:7.
35. Minamino T, MacNab RM. FliH, a soluble component of the type III flagellar export apparatus of Salmonella, forms a complex with FliI and inhibits its ATPase activity. Mol Microbiol. 2000; 37:1494–1503. [PubMed: 10998179]
36. Claret L, Calder SR, Higgins M, Hughes C. Oligomerization and activation of the FliI ATPase central to bacterial flagellum assembly. Mol Microbiol. 2003; 48:1349–1355. [PubMed: 12787361]
37. Pozidis C, Chalkiadaki A, Gomez-Serrano A, Stahlberg H, Brown I, Tampakaki AP, Lustig A, Sianidis G, Politou AS, Engel A, Panopoulos NJ, Mansfield J, Pugsley AP, Karamanou S,

Economou A. Type III protein translocase: HrcN is a peripheral ATPase that is activated by oligomerization. J Biol Chem. 2003; 278:25816–25824. [PubMed: 12734178]

38. Ibuki T, Imada K, Minamino T, Kato T, Miyata T, Namba K. Common architecture of the flagellar type III protein export apparatus and F- and V-type ATPases. Nat Struct Mol Biol. 2011; 18:277–282. [PubMed: 21278755]
39. Evans LD, Stafford GP, Ahmed S, Fraser GM, Hughes C. An escort mechanism for cycling of export chaperones during flagellum assembly. Proc Natl Acad Sci U S A. 2006; 103:17474–17479. [PubMed: 17088562]
40. Auvray F, Ozin AJ, Claret L, Hughes C. Intrinsic membrane targeting of the flagellar export ATPase FliI: interaction with acidic phospholipids and FliH. J Mol Biol. 2002; 318:941–950. [PubMed: 12054792]
41. Gonzalez-Pedrajo B, Fraser GM, Minamino T, Macnab RM. Molecular dissection of Salmonella FliH, a regulator of the ATPase FliI and the type III flagellar protein export pathway. Mol Microbiol. 2002; 45:967–982. [PubMed: 12180917]
42. Formal SB, Dammin GJ, Labrec EH, Schneider H. Experimental Shigella infections: characteristics of a fatal infection produced in guinea pigs. J Bacteriol. 1958; 75:604–610. [PubMed: 13538931]
43. Jouihri N, Sory MP, Page AL, Gounon P, Parsot C, Allaoui A. MxiK and MxiN interact with the Spa47 ATPase and are required for transit of the needle components MxiH and MxiI, but not of Ipa proteins, through the type III secretion apparatus of Shigella flexneri. Mol Microbiol. 2003; 49:755–767. [PubMed: 12864857]
44. Whitmore L, Wallace BA. Protein secondary structure analyses from circular dichroism spectroscopy: methods and reference databases. Biopolymers. 2008; 89:392–400. [PubMed: 17896349]
45. Andrade MA, Chacon P, Merelo JJ, Moran F. Evaluation of secondary structure of proteins from UV circular dichroism spectra using an unsupervised learning neural network. Protein Eng. 1993; 6:383–390. [PubMed: 8332596]
46. Lebowitz J, Lewis MS, Schuck P. Modern analytical ultracentrifugation in protein science: a tutorial review. Protein Sci. 2002; 11:2067–2079. [PubMed: 12192063]
47. Laue, T., Shah, B., Ridgeway, T., Pelletier, S. Analytical Ultracentrifugation in Biochemistry and Polymer Science. In: Harding, S.Rowe, A., Horton, JC., editors. Analytical Ultracentrifugation in Biochemistry and Polymer Science. Royal Society of Chemistry; United Kingdom: 1992.
48. Sansonetti PJ, Ryter A, Clerc P, Maurelli AT, Mounier J. Multiplication of Shigella flexneri within HeLa cells: lysis of the phagocytic vacuole and plasmid-mediated contact hemolysis. Infect Immun. 1986; 51:461–469. [PubMed: 3510976]
49. Niesel DW, Chambers CE, Stockman SL. Quantitation of HeLa cell monolayer invasion by Shigella and Salmonella species. J Clin Microbiol. 1985; 22:897–902. [PubMed: 4066921]
50. Imada K, Minamino T, Tahara A, Namba K. Structural similarity between the flagellar type III ATPase FliI and F1-ATPase subunits. Proc Natl Acad Sci U S A. 2007; 104:485–490. [PubMed: 17202259]
51. Minamino T, Kazetani K, Tahara A, Suzuki H, Furukawa Y, Kihara M, Namba K. Oligomerization of the bacterial flagellar ATPase FliI is controlled by its extreme N-terminal region. J Mol Biol. 2006; 360:510–519. [PubMed: 16780875]
52. Minamino T, Tame JR, Namba K, Macnab RM. Proteolytic analysis of the FliH/FliI complex, the ATPase component of the type III flagellar export apparatus of Salmonella. J Mol Biol. 2001; 312:1027–1036. [PubMed: 11580247]
53. Galan JE, Lara-Tejero M, Marlovits TC, Wagner S. Bacterial type III secretion systems: specialized nanomachines for protein delivery into target cells. Annu Rev Microbiol. 2014; 68:415–438. [PubMed: 25002086]
54. Kane KA, Dorman CJ. VirB-mediated positive feedback control of the virulence gene regulatory cascade of Shigella flexneri. J Bacteriol. 2012; 194:5264–5273. [PubMed: 22821978]
55. Maurelli AT, Sansonetti PJ. Identification of a chromosomal gene controlling temperature-regulated expression of Shigella virulence. Proc Natl Acad Sci U S A. 1988; 85:2820–2824. [PubMed: 3282241]

56. Stensrud KF, Adam PR, La Mar CD, Olive AJ, Lushington GH, Sudharsan R, Shelton NL, Givens RS, Picking WL, Picking WD. Deoxycholate interacts with IpaD of Shigella flexneri in inducing the recruitment of IpaB to the type III secretion apparatus needle tip. J Biol Chem. 2008; 283:18646–18654. [PubMed: 18450744]
57. Olive AJ, Kenjale R, Espina M, Moore DS, Picking WL, Picking WD. Bile salts stimulate recruitment of IpaB to the Shigella flexneri surface, where it colocalizes with IpaD at the tip of the type III secretion needle. Infect Immun. 2007; 75:2626–2629. [PubMed: 17296762]
58. Epler CR, Dickenson NE, Olive AJ, Picking WL, Picking WD. Liposomes recruit IpaC to the Shigella flexneri type III secretion apparatus needle as a final step in secretion induction. Infect Immun. 2009; 77:2754–2761. [PubMed: 19433542]
59. Dickenson NE, Arizmendi O, Patil MK, Toth RTt, Middaugh CR, Picking WD, Picking WL. N-terminus of IpaB provides a potential anchor to the Shigella type III secretion system tip complex protein IpaD. Biochemistry. 2013; 52:8790–8799. [PubMed: 24236510]
60. Dickenson NE, Zhang L, Epler CR, Adam PR, Picking WL, Picking WD. Conformational changes in IpaD from Shigella flexneri upon binding bile salts provide insight into the second step of type III secretion. Biochemistry. 2011; 50:172–180. [PubMed: 21126091]
61. Morita-Ishihara T, Ogawa M, Sagara H, Yoshida M, Katayama E, Sasakawa C. Shigella Spa33 is an essential C-ring component of type III secretion machinery. J Biol Chem. 2006; 281:599–607. [PubMed: 16246841]
62. Imada K, Minamino T, Uchida Y, Kinoshita M, Namba K. Insight into the flagella type III export revealed by the complex structure of the type III ATPase and its regulator. Proc Natl Acad Sci U S A. 2016; 113:3633–3638. [PubMed: 26984495]
63. Bai F, Morimoto YV, Yoshimura SD, Hara N, Kami-Ike N, Namba K, Minamino T. Assembly dynamics and the roles of FliI ATPase of the bacterial flagellar export apparatus. Sci Rep. 2014; 4:6528. [PubMed: 25284201]
64. Diepold A, Sezgin E, Huseyin M, Mortimer T, Eggeling C, Armitage JP. A dynamic and adaptive network of cytosolic interactions governs protein export by the T3SS injectisome. Nat Commun. 2017; 8:15940. [PubMed: 28653671]

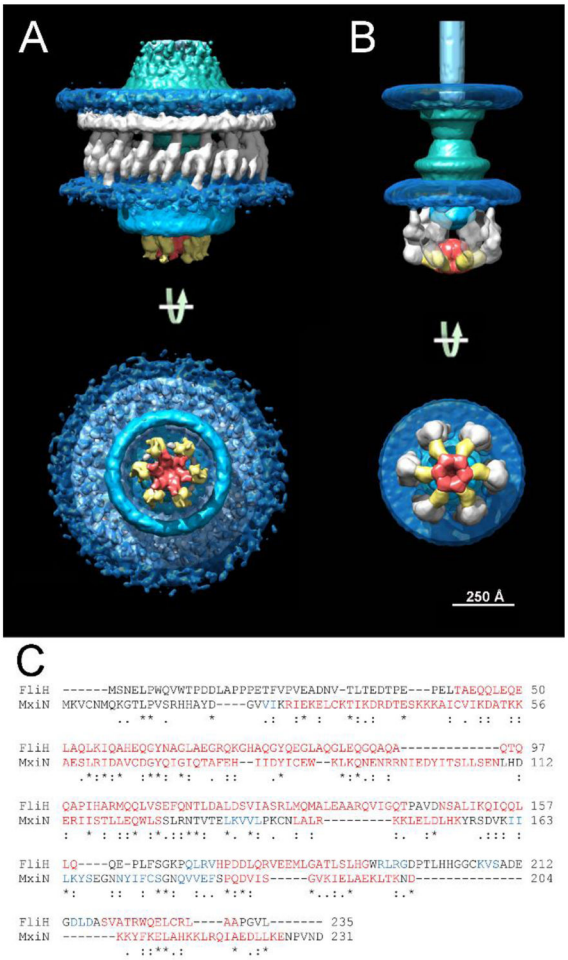

Figure 1. Comparison of cryo-electron tomography maps of A) the *Helicobacter pylori* flagellar secretion system and B) the *Shigella flexneri* T3SS sorting platform

The ATPases FliI and Spa47 are positioned similarly at the base of the *Helicobacter* flagellar motor and *Shigella* T3SS platforms, respectively (red). The flagellar FliI inhibitor, FliH, and the putative *Shigella* FliH homolog, MxiN, are colored yellow and are both seen extending from their respective ATPases. **C)** Sequence alignment of FliH (UniProt accession number P15934) and MxiN (UniProt accession number Q6XVX6) was performed with the UniProt sequence alignment tool, Clustal Omega.[1] Fully conserved residues (*), conservation between groups with strongly similar properties (:), and weakly similar properties (.) are identified. α-helical and β-sheet regions, as predicted by the PSIPRED structure prediction server,[2] are color-coded red and blue within the sequences, respectively. Three-dimensional electron density structures were generated using the UCSF software package Chimera[4] and the previously published coordinates from EMDB-8459 and EMDB-2667 for the flagellar secretion system[6] and *Shigella* T3SS sorting platform,[7] respectively.

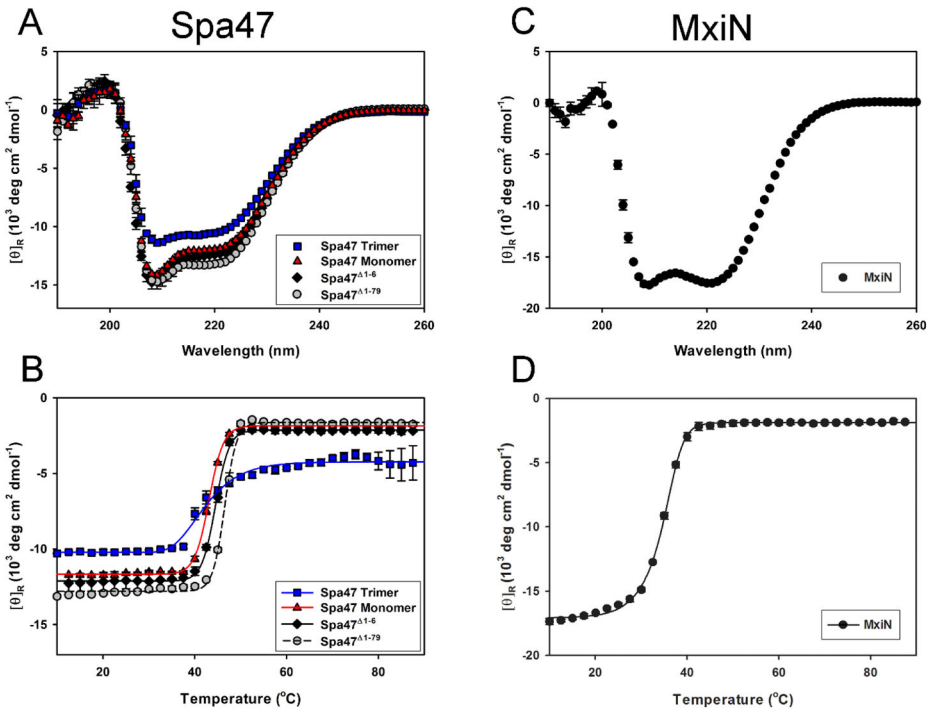

Figure 2. Analysis of secondary structure content and stability of Spa47 and MxiN

A) Far-UV CD spectra of monomeric and trimeric Spa47, Spa47$^{\Delta 1\text{-}6}$, and Spa47$^{\Delta 1\text{-}79}$ all contain minima at 208 and 222 nm, consistent with predominantly α-helical secondary structures. **B)** Thermal unfolding of the secondary structures of each tested Spa47 constructs is observed by plotting the mean residue molar ellipticity at 222 nm while the protein solutions are heated from 10 to 90 °C. **C)** and **D)** represent a CD spectrum and thermal unfolding profile for MxiN, respectively. The displayed data is plotted as the mean ± standard deviation from three measurements.

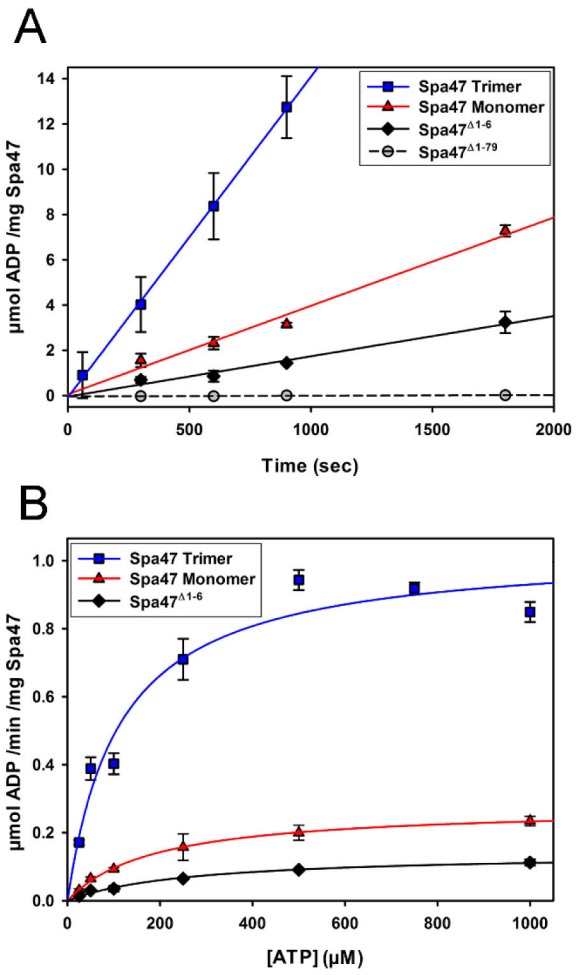

Figure 3. The N-terminus of Spa47 is essential for proper activation

A) An α-^{32}P-ATP hydrolysis assay shows that isolated monomeric and trimeric Spa47 are both active, with the trimer resulting in a significantly higher rate of hydrolysis compared to the monomer. Spa47$^{\Delta 1\text{-}79}$ is completely inactive, resulting in background levels of ATP hydrolysis. The newly engineered Spa47$^{\Delta 1\text{-}6}$ construct is minimally active, with an ATP hydrolysis rate between those of the isolated Spa47 monomer and Spa47$^{\Delta 1\text{-}79}$. **B)** Substrate concentration-dependence of ATPase activity was tested for full-length Spa47 monomer and trimer and for the Spa47$^{\Delta 1\text{-}6}$ construct by plotting initial reaction velocities as a function of substrate (ATP) concentration. The data were fit to the Michaelis-Menten equation to determine the kinetic parameters K_M, V_{max}, k_{cat}, and k_{cat}/K_M (see Table 2). All presented data points represent the mean ± standard deviation from three independent analyses.

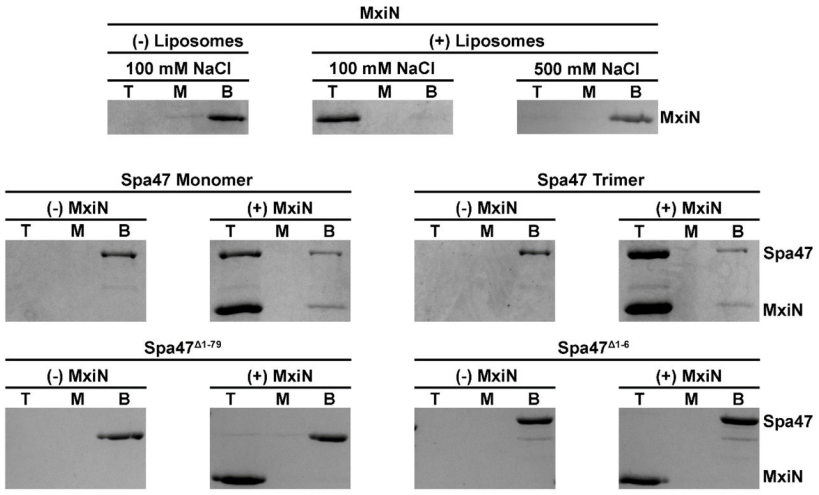

Figure 4. The N-terminus of Spa47 is required for interaction with MxiN

The presence of protein in top (T), middle (M), and bottom (B) fractions of a sucrose gradient following centrifugation with asolectin liposomes was determined by SDS–PAGE. MxiN was found in the top fraction of the gradient following centrifugation with liposomes under low salt conditions (100 mM NaCl). MxiN remained in the bottom fraction under moderate salt conditions (500 mM NaCl), indicative of a peripheral interaction between MxiN and the asolectin liposomes. Monomeric and trimeric full-length Spa47 and the N-terminal truncation constructs Spa47$^{\Delta 1\text{-}79}$ and Spa47$^{\Delta 1\text{-}6}$ remained in the bottom fraction in the presence of liposomes while both monomeric and trimeric Spa47 “floated” to the top fraction when incubated with liposomes and MxiN. Neither the Spa47$^{\Delta 1\text{-}79}$ nor Spa47$^{\Delta 1\text{-}6}$ constructs interacted with MxiN, remaining in the bottom fractions while MxiN independently moved to the top fraction.

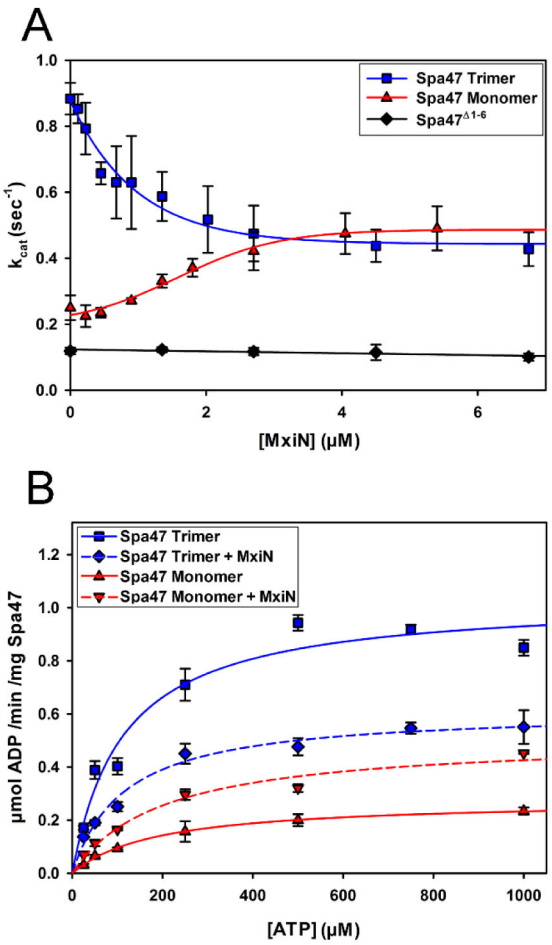

Figure 5. MxiN differentially regulates the activity of monomeric and oligomeric Spa47

A) The effect of MxiN on Spa47 activity was tested for the full-length monomeric and trimeric Spa47 and Spa47$^{\Delta 1\text{-}6}$. Trimeric Spa47 activity decreased with MxiN concentration while the monomeric Spa47 activity increased with increasing concentrations of MxiN. The activity of the Spa47$^{\Delta 1\text{-}6}$ construct was unaffected by MxiN. **B)** The effect of MxiN on Spa47 substrate concentration-dependence was tested by plotting initial reaction velocities as a function of substrate (ATP) concentration in the absence and presence of saturating concentrations of MxiN and fitting the data to the Michaelis-Menten equation. All data points are presented as the mean ± standard deviation from three independent analyses.

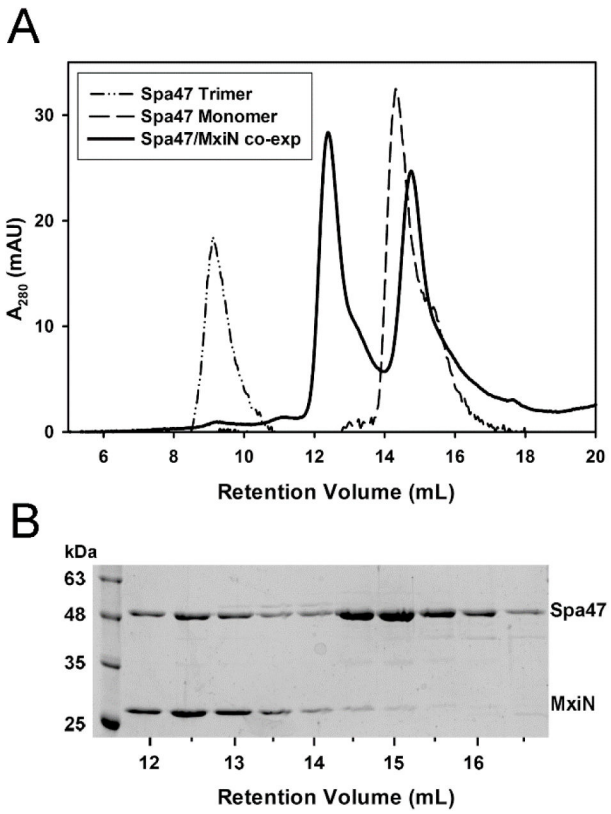

Figure 6. MxiN interacts with Spa47 *in vivo*

Co-expressed Spa47 and MxiN were purified from *E. coli* and analyzed by size exclusion chromatography. **A)** The A_{280} size exclusion chromatogram and **B)** the corresponding SDS-PAGE gel of the eluted fractions identify a MxiN/Spa47 complex that elutes from sizing at ~12.5 mL, between the retention volumes observed for the isolated 47.6 kDa Spa47 monomer (~15 mL) and trimer (~9 mL). Unbound Spa47 monomer elutes at ~15 mL. The monomer MW of MxiN is 28.9 kDa.

Table 1

Circular Dichroism Analysis of MxiN and Spa47 N-terminal Truncation Constructs

	Percent Secondary Structure[a] (% ± SD)			
	α-Helix	β-Sheet	Random Coil	Tm[b] (°C ± SD)
Spa47 Trimer	34 ± 1	22 ± 1	44 ± 1	40.2 ± 0.7
Spa47 Monomer	40 ± 2	21 ± 1	39 ± 2	42.8 ± 0.2
$Spa47^{\Delta 1\text{-}6}$	43 ± 4	19 ± 1	39 ± 4	45.3 ± 0.2
$Spa47^{\Delta 1\text{-}79}$	48 ± 1	19 ± 1	34 ± 1	47.8 ± 0.4
MxiN	59 ± 1	8 ± 1	33 ± 0	35.6 ± 0.3

[a] Secondary structure content analysis of far-UV CD spectra was performed using the Dichroweb software package K2D. The determined percent α-helix, β-sheet, and random coil are reported for monomeric and trimeric Spa47, $Spa47^{\Delta 1\text{-}6}$, $Spa47^{\Delta 1\text{-}79}$, and MxiN.

[b] Secondary structure thermal stability was tested by measuring CD signal at 222 nm while increasing the solution temperature from 10 to 90 °C.

All results are reported as the mean ± standard deviation from three independent analyses.

Table 2

Effect of Oligomerization and MxiN Interaction on Spa47 Kinetics

Spa47 Construct[a]	K_M (μM)	V_{max} (μmol min^{-1} mg^{-1})	k_{cat} (sec^{-1})	k_{cat}/K_M (M^{-1} sec^{-1})
Spa47 Monomer	181 ± 30	0.28 ± 0.01	0.22 ± 0.01	1.3 ± 0.2 x 10^3
Spa47 Trimer	114 ± 20	1.04 ± 0.02	0.84 ± 0.01	7.5 ± 1.2 x 10^3
$Spa47^{\Delta 1\text{-}6}$	269 ± 31	0.14 ± 0.01	0.11 ± 0.01	4.2 ± 0.3 x 10^2
Spa47 Monomer + MxiN	201 ± 8	0.51 ± 0.01	0.41 ± 0.01	2.1 ± 0.1 x 10^3
Spa47 Trimer + MxiN	116 ± 19	0.62 ± 0.06	0.50 ± 0.05	4.4 ± 0.3 x 10^3

[a] Initial reaction velocity was measured as a function of substrate (ATP) concentration for each listed Spa47 constructs and the results fit to the Michaelis-Menten equation to determine the apparent K_M, V_{max}, k_{cat}, and k_{cat}/K_M for each condition.

All values are presented as the mean ± standard deviation of three independent analyses. Statistical analysis was performed for each kinetic parameter using a one-way ANOVA followed by a Dunnett's post test ($p \leq 0.05$). All differences among V_{max} and k_{cat} values are significant. All differences in K_M values except those between (Spa47 Monomer and Spa47 Monomer + MxiN) and (Spa47 Trimer and Spa47 Trimer + MxiN) are significant. All differences in k_{cat}/K_M are significant except those between (Spa47 Monomer and $Spa47^{\Delta 1\text{-}6}$) and (Spa47 Monomer and Spa47 Monomer + MxiN).

Table 3

Effect of engineered N-terminal Spa47 Truncations on *Shigella* Virulence Phenotype

***Shigella* Strain**	**Hemolysis[a](% ± SD)**	**Invasion[b](% ± SD)**
Spa47 Complement	100	100
Spa47 null	3 ± 0	0 ± 0
Spa47$^{\Delta 1\text{-}79}$ Complement	3 ± 0	0 ± 0
Spa47$^{\Delta 1\text{-}6}$ Complement	100 ± 6	89 ± 19

[a]The ability of *Shigella* strains expressing Spa47$^{\Delta 1\text{-}6}$ and Spa47$^{\Delta 1\text{-}79}$ to lyse red blood cells was tested using a hemolysis assay that spectrophotometrically quantifies the release of hemoglobin from erythrocytes.

[b]The ability of the tested *Shigella* strains to invade cultured HeLa cells was measured by a standard gentamicin protection assay.

Hemolysis and invasion results are presented as the percent ± standard deviation relative to the *S. flexneri* strain expressing wild-type Spa47. (n = 3 independent measurements)